

Synoptic and dynamic aspects of an extreme springtime Saharan dust outbreak

By PETER KNIPPERTZ^{1*} and ANDREAS H. FINK²

¹*Department of Atmospheric & Oceanic Sciences, University of Wisconsin–Madison, USA*

²*Institute of Geophysics and Meteorology, University of Cologne, Germany*

(Received 31 May 2005; revised 20 October 2005)

SUMMARY

In March 2004, a large-scale, strong and persistent outbreak of Saharan dust on to the adjacent tropical and subtropical Atlantic Ocean was observed in satellite imagery. Surface observations show that the event was accompanied by unusual weather conditions across large parts of North Africa including low temperatures and strong winds over the Sahara, extreme precipitation in Libya and a heat wave on the Guinea coast. The dust outbreak was associated with an unseasonally southerly position of the Intertropical Convergence Zone and a delayed northward progression of the African monsoon.

The dust front was initially related to a density current caused by strong evaporational cooling along a precipitating cloud-band that penetrated into the northern Sahara ahead of an upper-level trough. At later stages, massive upper-level convergence, sinking, low-level divergence and an explosive anticyclogenesis over north-west Africa caused strong northerly flow and a quick spreading of the dust front to the south and west. The strong pressure gradients over North Africa were further enhanced by the formation of a cyclone ahead of the upper-trough. A dynamical analysis based on potential-vorticity (PV) theory provides new insights into the generation of North African harmattan surges. Using a PV inversion, it is shown that the explosive anticyclogenesis was caused largely by unbalanced dynamics related to the density current, divergent outflow from the precipitation over Libya and inertial instability in the entrance region of the strong subtropical jet and tropical plume along the eastern side of the upper trough. These processes enhanced the effects of the balanced advection of negative vorticity and cold air by the large-scale wave. Moreover, we show the importance of an explosive cyclogenesis event over the central North Atlantic for the amplification of the downstream wave associated with the penetration of the cold front into North Africa.

KEYWORDS: Density current Harmattan surge Potential vorticity Precipitation Subtropical jet Tropical plume Unbalanced dynamics

1. INTRODUCTION

On 4 March 2004 images from the visible (VIS) channel of the Meteosat 7 satellite (Fig. 1(a)) show a huge, dense, meridionally oriented dust plume off the north-west African coast reaching from west of Madeira to Cape Verde†. This plume spreads laterally, moves westward and by 12 UTC 6 March forms an arc more than 5000 km long from Guinea to the northern tip of Morocco (Fig. 1(b)). At the same time, a more zonally oriented dust front is evident over the Gulf of Guinea. The following analysis examines the synoptic evolution and the dynamic processes involved in this extraordinary dust outbreak over Africa.

The Sahara desert is the most prominent global source of aeolian dust (Prospero *et al.* 2002; Washington *et al.* 2003). Airborne dust has impacts on (a) the atmospheric radiation budget and thereby vertical stability, (b) on cloud microphysics by providing condensation nuclei, (c) on marine biochemistry by providing nutrients to algae and corals and (d) on the living conditions of people inhabiting the Sahara and its surroundings by affecting visibility, air traffic and human health. Satellite-based climatological studies have demonstrated that dust exports from the Sahara take place in discrete outbreaks of several days' duration and that their location and direction shift with the seasonal movement of the Intertropical Convergence Zone (ITCZ) (Jankowiak and Tanré 1992; Swap *et al.* 1996; Moulin *et al.* 1997). The annual peak in outbreak activity usually

* Corresponding author: Institut für Physik der Atmosphäre, Johannes Gutenberg-Universität Mainz, Becherweg 21, D-55099 Mainz, Germany. e-mail: knippertz@uni-mainz.de

† For geographical terms used throughout the text refer to Fig. 2, and for abbreviations of station names to Table 1.

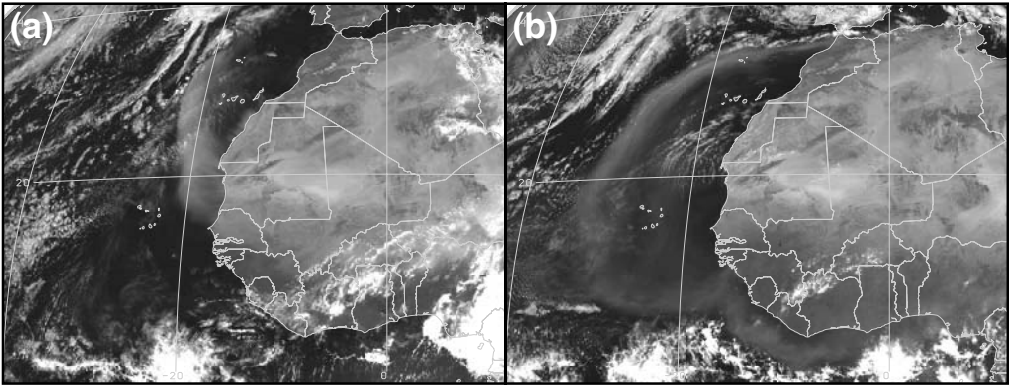


Figure 1. Meteosat 7 VIS satellite images for 12 UTC: (a) 4 March 2004 and (b) 6 March 2004.

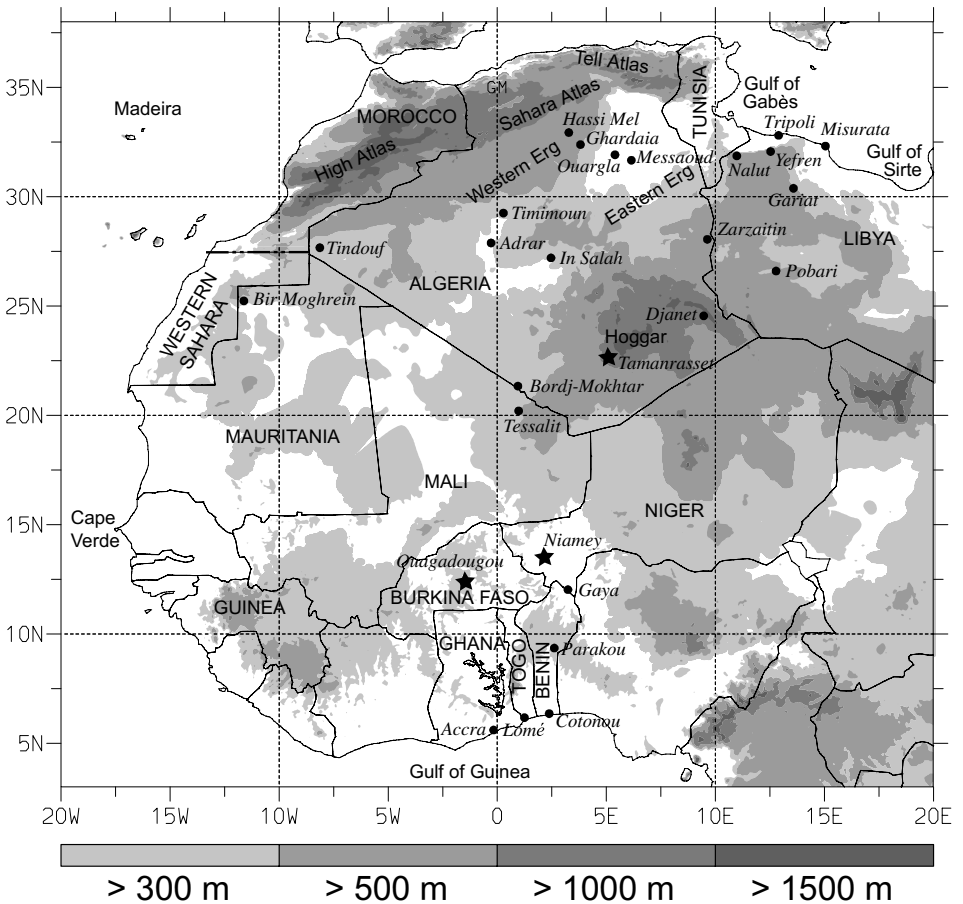


Figure 2. Map of North Africa with geographical terms. The grey scale shows terrain height above mean sea level (m). Synoptic and upper-air stations employed in this study are indicated by dots and stars, respectively. The abbreviations of station names are set out in Table 1.

TABLE 1. ABBREVIATIONS USED FOR STATION NAMES IN TEXT AND FIGURE 3

Abbreviation	Station name	Abbreviation	Station name	Abbreviation	Station name
AD	Adrar	BI	Bir Moghreïn	BO	Bordj-Mokhtar
DJ	Djanet	HM	Hassi Mel	IS	In Salah
MS	Messaoud	NL	Nalut	OU	Ouargla
PB	Pobari	TD	Tindouf	TM	Timimoun
TS	Tessalit	ZA	Zarzaitin		

occurs in late winter and spring (Swap *et al.* 1996). Large-scale processes, such as the North Atlantic Oscillation and Sahelian rainfall, control the interannual variability of the dust export to the Atlantic and Mediterranean regions (Chiapello and Moulin 2002; Ginoux *et al.* 2004; Chiapello *et al.* 2005; Evan *et al.* 2006). In the cool season, dust is frequently transported from the Sahara to the Gulf of Guinea in the harmattan, and to the tropical Atlantic and South America (Prospero and Carlson 1981). Occasional strong dust outbreaks have been documented over the subtropical Atlantic (Jankowiak and Tanré 1992), the Canary Islands (Cana 2002), the central Mediterranean Sea (Prodi and Fea 1979; Alpert and Ganor 1993) and even Fennoscandia (Franzén *et al.* 1995), usually in connection with the penetration of an upper-level trough to low latitudes. Some authors have observed a relation between dust storms and low-level cold fronts, their associated jets, tropopause folds and stratospheric intrusions (Danielsen 1975; Alpert and Ganor 1993). Studying a strong harmattan, Kalu (1979) documented a sudden intensification of the subtropical anticyclone in association with a pressure surge over the Sahara, high low-level wind speeds and a cold outbreak from the Mediterranean Sea. Washington and Todd (2005) revealed a relation between an intensification of the Libyan anticyclone and dustiness over the Bodélé Depression in Chad. Low vertical stability over the Sahara allows a downward mixing of high-momentum air to the surface and an upward mixing of dust which supports both its mobilization and displacement (Danielsen 1975; Prodi and Fea 1979; Thorncroft and Flocas 1997, TF97 hereafter). The last of these authors used potential vorticity (PV) to diagnose a cyclogenesis in the lee of the Atlas Mountains associated with dust storms in the Sahara.

The remainder of the paper is organized as follows: after describing, in section 2, the observational data used, we focus on the synoptic evolution and chronology of significant changes in surface and upper-air weather conditions associated with the dust storm (section 3). In section 4, we examine the large-scale flow fields before and during the event, followed by a PV-based analysis of the balanced and unbalanced dynamic processes involved (section 5). The paper concludes with a summary and discussion in section 6.

2. DATA

For the analysis which follows, we used synoptic surface (SYNOP) and radiosonde (TEMP) observations from various stations in Africa distributed by the World Meteorological Organization (WMO). In addition, hourly METAR surface observations from major airports proved to be helpful in delineating the progression of the dust front. The National Meteorological Services of Niger and Benin provided hard copies of detailed instrumental and eye observations, taken at selected synoptic stations within their networks, or complemented missing SYNOP reports. Finally, various meteorological data from the IMPETUS* network were available for locations in central and southern Benin,

* 'An integrated approach to the efficient management of scarce water resources in West Africa'.

and southern Niger. The parameters used were 15-minute averages of temperature, humidity, and pressure, as well as 10-minute averages of short- and long-wave incident and outgoing radiation, all measured at a height of 2 m, and wind speed and direction at an altitude of 10 m. Surface weather information (fronts, pressure systems) was taken from twice-daily weather charts published by the German Weather Service (DWD).

Standard Meteosat 7 infrared (IR) and VIS satellite images were obtained through the Space Science and Engineering Center of the University of Wisconsin in Madison, USA. In order to visualize the dust over land as well as possible, we used Meteosat Second Generation (MSG) images that were produced from a combination of three IR channels: blue, channel 9 ($10.8 \mu\text{m}$); red, channel 9 minus channel 10 ($12 \mu\text{m}$); green, channel 9 minus channel 7 ($8.7 \mu\text{m}$). The images were taken from the EUMETSAT home page* and converted to grey scale. The large-scale circulation is represented by twice-daily (00 and 12 UTC) European Centre for Medium-Range Weather Forecasts (ECMWF) Tropical Ocean and Global Analysis (TOGA) data with $2.5^\circ \times 2.5^\circ$ grid spacing on standard pressure levels (Trenberth 1992). It is emphasized that Morocco, Tunisia and especially Algeria have a remarkably dense and reliable network of eight radiosonde stations along the coast and in the Algerian Sahara. Five PILOT low-level wind stations, three of which are located in the northern Algerian Sahara, augment this network. In a set of data denial experiments using the ECMWF 4D-Var analysis system, Tompkins *et al.* (2005) showed that for the African easterly jet even a coarse network of conventional platforms such as radiosondes and pilot balloons was more important than other sources of information. Thus, we are confident that the three-dimensional ECMWF analysis fields provide a reasonable description of the dynamics and thermodynamics of the event. The General Meteorological Package (GEMPAK) has been employed for data interpolation (e.g. to isentropic levels), and the computation and display of streamlines and other meteorological parameters (e.g. PV).

3. SYNOPTIC OBSERVATIONS

(a) *Evolution of the dust outbreak*

For the 24-hour period ending 18 UTC 3 March 2004, Fig. 3 shows 6-hourly MSG images with superimposed station observations. At 18 UTC 2 March, a thick dust front with a sharp leading edge is evident over central Algeria (thick line in Fig. 3(a)). The nearby synoptic station Adrar (AD hereafter; for station locations and abbreviations, see Fig. 2 and Table 1) reported a temperature drop from 25°C to 12°C , a dew point rise from -11°C to $+1^\circ\text{C}$ and a pressure rise of 4.3 mb over the previous 3 hours, as well as north-easterly winds of 36 knots and a visibility reduced to 100 m by moderate dust storm (Fig. 3(a)). MSG images around 14 UTC reveal that the dust front initially emerges from the southern tip of a SW–NE oriented cloud band over the Great Western Erg, suggesting a dust mobilization in the alluvial plains south of the High and Sahara Atlas (not shown). This is corroborated by afternoon observations at Timimoun (TM). Underneath the cloud band, light rains of up to 1 mm were recorded between 06 and 18 UTC 2 March at several oases in north-eastern Algeria. The strong northerly winds in the lee of the Sahara Atlas, e.g. at Hassi Mel (HM), indicate a föhn situation (Fig. 3(a)).

Light to intermediate rains over and to the north of the Great Eastern Erg continued during the night, while the winds in the area settled somewhat (e.g. Ouargla (OU) at 00 UTC 3 March; Fig. 3(b)). Simultaneously, the arched dust front reached northern

* <http://www.eumetsat.int>

Mauritania and Mali and became clearly detached from the clouds over north-eastern Algeria. This development continued and, shortly before 06 UTC, the dust plume passed the central Saharan station Bordj-Mokhtar (BO) that reported a dust storm with low visibility at this time (Fig. 3(c)). In the course of 3 March, rains in north-eastern Algeria and southern Tunisia intensified. Messaoud (MS, Fig. 3(c)) and OU (Fig. 3(d)) reported moderate rain at 06 and 12 UTC 3 March, respectively, with the latter station recording 12 mm during this period. When the rains finally shifted into north-western Libya, precipitation intensified dramatically, resulting in 24 hour accumulations of 115 mm at Gariat, 62 mm at Misurata and 41 mm at Tripoli (Tarabulus) by 06 UTC 4 March (not shown). For the entire month of March 2004, Yefren reported a rainfall total of 101 mm, but only three days with more than 1 mm of accumulated precipitation. Even though the SYNOP reports are incomplete for this month, the existing information points to the fact that most of the 101 mm fell during 3 and 4 March. According to Griffiths and Soliman (1972), a rainfall of 115 mm at Gariat is about three times the average *annual* rainfall there.

These rainfalls were accompanied by a second intensification in the low-level northerlies and widespread dust storm conditions in the Algerian Sahara as seen from the SYNOPs at In Salah (IS), Zarzaitin (ZA) and Tindouf (TD) with mean winds of about 30 knots at 12 UTC 3 March (Fig. 3(d)). At the same time, Ghardaia reported a dust storm and visibility of 500 m (not shown). At 18 UTC, strong north-easterly winds were measured in north-western Libya, e.g. 48 knots at Nalut (NL), and dust storms were observed at many stations in the western and central Sahara Desert (Fig. 3(e)). While the extreme winds of up to 65 knots at the highly exposed station Bir Moghrein (BI, Fig. 3(d)) on that day were associated with the passage of the sharp leading edge of the dust front (thick black line), the blowing dust at BI, Tessalit (TS), TM, Djanet (DJ) and Pobari (PB) 12 hours later clearly occurred behind this front, where the MSG dust signal was weaker (Fig. 3(e)). At 18 UTC the dust formed an almost circular arc from the Western Saharan coast across Mauritania and Mali into Niger where it disappeared under a cloud band that will be further discussed in subsection 5(c).

As shown in Fig. 1, the dust front continued to spread southwards and westwards during the following days. It passed the Cape Verde Islands at 18–21 UTC 4 March and the Guinea Coast around 06 UTC on the next day. Data from weather and research stations in Niger, Burkina Faso and Benin reflect the impressive weather conditions associated with the frontal passage. At the central Sahelian station Niamey the dust front passed around 0230 UTC 4 March, accompanied by a reduction in visibility, a surge in the harmattan northerlies, relative humidity (RH) values below 10% and a 24-hour pressure rise of 6 mb, a remarkable value at this tropical latitude (not shown). The front reached Parakou about 15.5 hours later and caused pressure to rise 3.6 mb within 24 hours. On the day after the dust front passage (5 March) the station reported a RH value of 8% at 1335 UTC.

(b) Vertical structure

Soundings taken before and during the passage of the dust front were available for several radiosonde stations in the Sahara and Sahel, but not in the Soudano–Guinean zone. At Tamanrasset (1364 m) in the Hoggar, where the passage of the front occurred shortly after 06 UTC 03 March 2004, 12 UTC soundings on 2 March (dashed) and 3 March (solid) show dramatic cooling (warming) below (above) 700 mb (Fig. 4(a)). The available dew-point data indicate a very dry low-to-mid troposphere. Missing humidity values are probably the result of dryness beyond the sensor range of the radiosonde. At 18 UTC 3 March a surface RH of 10% was observed at this station.

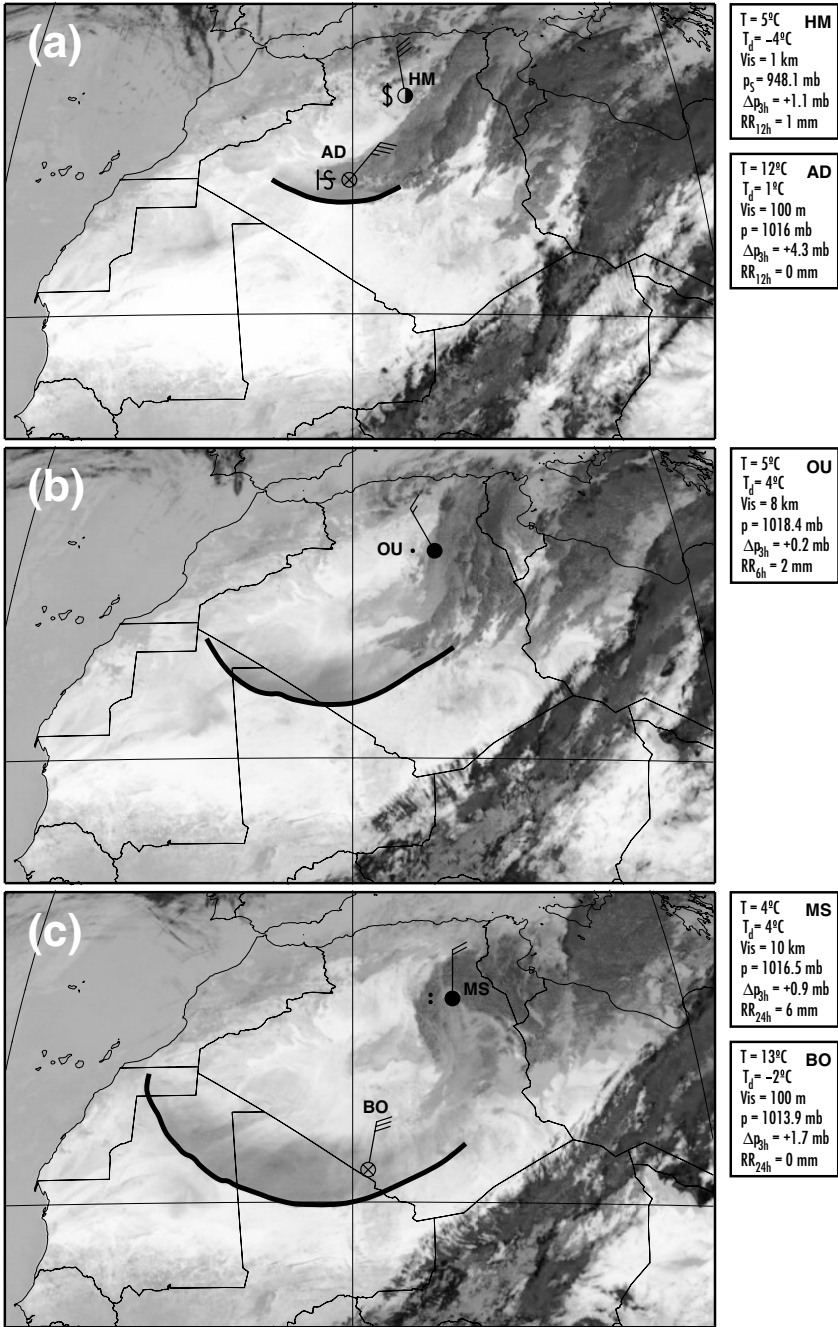


Figure 3. MSG satellite images at six-hourly intervals: (a) 18 UTC 2 March 2004; (b) 00 UTC 3 March; (c) 06 UTC 3 March; (d) 12 UTC 3 March and (e) 18 UTC 3 March 2004. For details on the shading see section 2 of the text. Selected station observations display wind at 2 m (half barb = 5 knots, full barb = 10 knots, triangle = 50 knots), cloud coverage (oktas; a cross indicates 'sky not visible') and significant weather (dots, commas and S's symbolize different intensities of rain, drizzle and dust storm, respectively; see WMO FM12 SYNOP code (WMO 1995) for details). The legends at the sides show temperature (T), dew point (T_d), visibility (Vis), pressure reduced to mean-sea-level p , station-level pressure p_s , 3 hourly (24 hourly for sub-Saharan stations) pressure tendency (Δp) and accumulated precipitation for the preceding 6, 12 or 24 hour period, respectively. The thick black line approximately marks the leading edge of the dust front. For station name abbreviations, see Table 1.

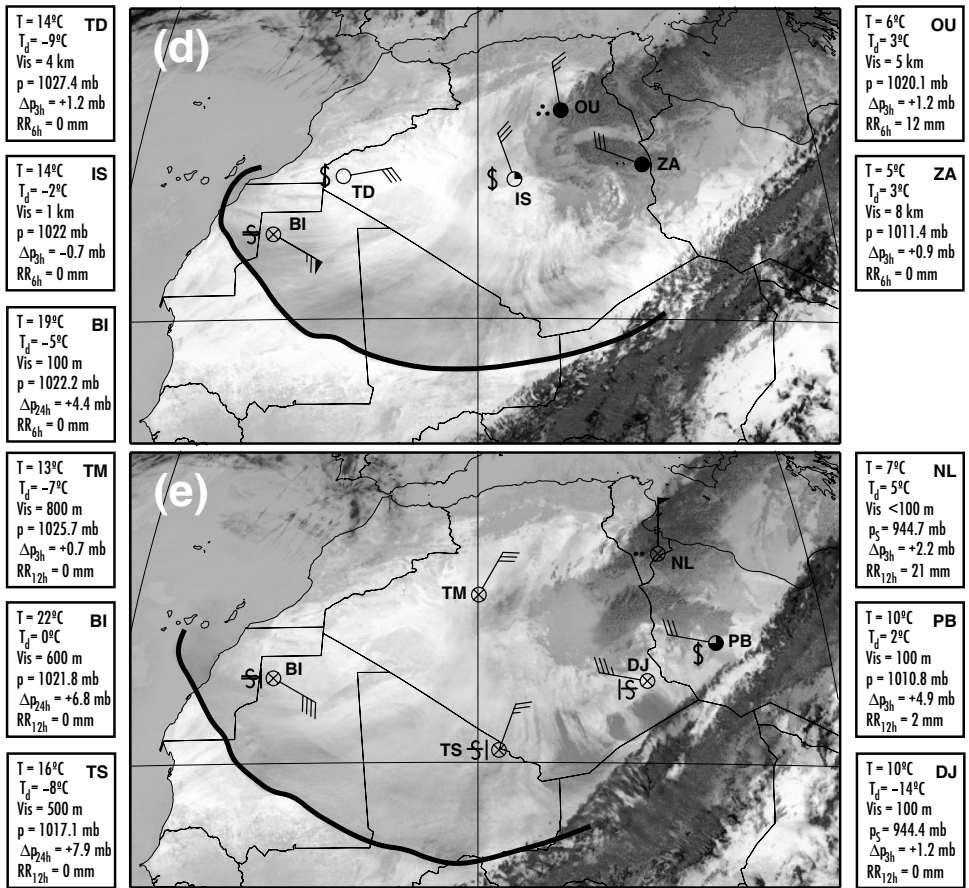


Figure 3. Continued.

Farther south, the warming aloft was less pronounced and the near-surface cooling occurred in a shallower layer reaching up to 800 mb, as revealed by a comparison between midday soundings on 3 and 4 March at Niamey (Fig. 4(b)). Similar temperature changes were observed at the radiosonde station Ouagadougou about 400 km WSW of Niamey (not shown). The thinning of the near-surface layer with a northerly flow of cool air is corroborated by backward trajectories from ECMWF analyses (not shown). The large dew-point depression in the Niamey sounding on 4 March corresponds to extreme RH values of less than 4% between the surface and 600 mb. The shallow low-level cool layer behind the dust front substantially reduces surface temperatures in the Sahelo-Soudanian zone. For example, at Gaya the maximum temperature is 37.0°C on 3 March and only 27.2°C the next day. Radiation measurements at Parakou, where the maxima on 3 and 5 March are 37.0°C and 30.6°C , respectively, show that the temperature drop was not simply the result of a dust-related reduction in global radiation, but that cold advection of extraordinary amplitude that late in the dry season must have occurred.

(c) *Heat wave and harmattan conditions at the Guinea coast*

The approach of the dust front to the Guinea Coast was associated with a heat wave and an unusually late and prolonged harmattan episode. On 4 March 2004, one day

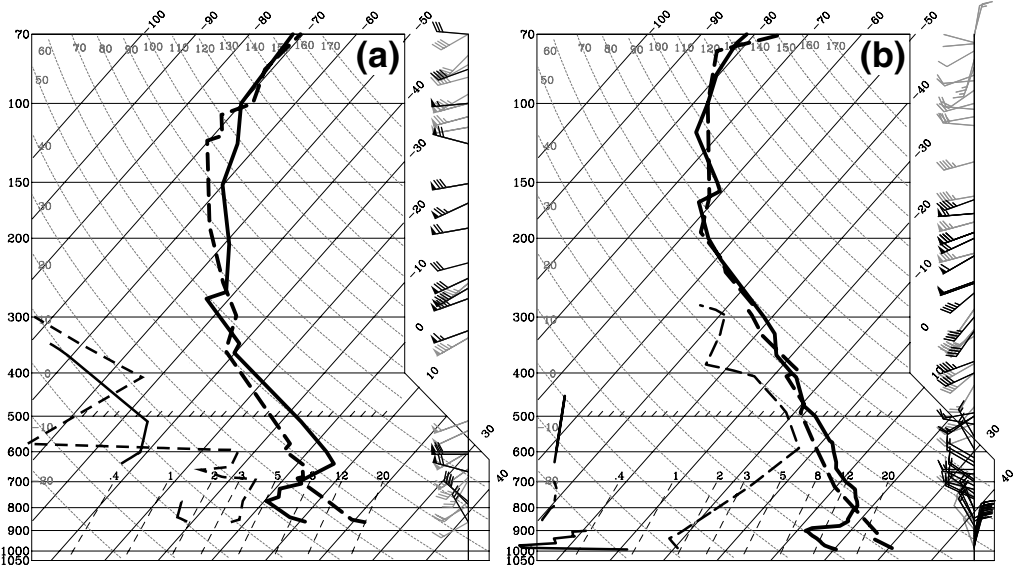


Figure 4. Skew T – $\log p$ diagrams for radio soundings from (a) Tamanrasset and (b) Niamey. Thick lines depict temperature and thin lines dew point. In (a) dashed lines and grey wind barbs are for 12 UTC 2 March 2004 and solid lines and black wind barbs are for 12 UTC 3 March. In (b) they are for 12 UTC on 3 and 4 March respectively. Wind barbs as in Fig. 3: half barb = 5 knots, full barb = 10 knots, triangle = 50 knots.

before the dust front crossed the coastline, temperature maxima reached 37.0°C at Cotonou and Accra, and 37.5°C even at Lomé. The reading at Cotonou exceeds the highest observed value during 1931–90 by 0.3°C . Measurements from Kipp and Zonen radiometers at the Cotonou airport gave high values of 10-minute global and 24-hour net radiation for this day (Fig. 5(b)). The smooth radiation curve in Fig. 5(b), as well as sunshine records and eye observations (not shown), on 4 March hint to an unusually clear morning sky and a below-average coverage of low clouds during the rest of the day. The suppressed cloud cover may be related to anomalous subsidence and a shoaling of the near-surface monsoon layer. The former is corroborated by ECMWF backward trajectories starting from near the surface (not shown). However, since even higher short-wave radiative forcing was observed both earlier and later during the first three weeks of March (Fig. 5(a)), additional factors must have contributed to the extreme temperatures.

Figure 6 shows observations of temperature, RH, visibility and 24-hour pressure tendency at Cotonou. In the climatological mean, low-level monsoonal south-westerlies blowing into the continental heat-low at 11 – 13°N are well developed and persistent along the Guinea coast at this time of the year. Often superimposed on the monsoon flow is the early morning development of an inland-moving sea-breeze convergence, causing a regular, cooling, daytime onshore wind from the Gulf of Benin, with sea-surface temperatures of about 28 – 29°C . On 4 March 2004, however, northerly offshore winds prevailed until 13 UTC and temperatures rose to 37°C (Fig. 6). When the wind subsequently veered to an onshore flow at 15 UTC, the temperature fell to 33°C . The unusual strong surface pressure rise observed at stations near the climatological zonal heat-low axis (e.g. Niamey and Parakou, subsection 3(a)) indicates that the absence of the cooling monsoon flow was related to the swift transfer of the continental heat-low on to the Gulf of Guinea in the course of 4 March. These observations indicate two causes

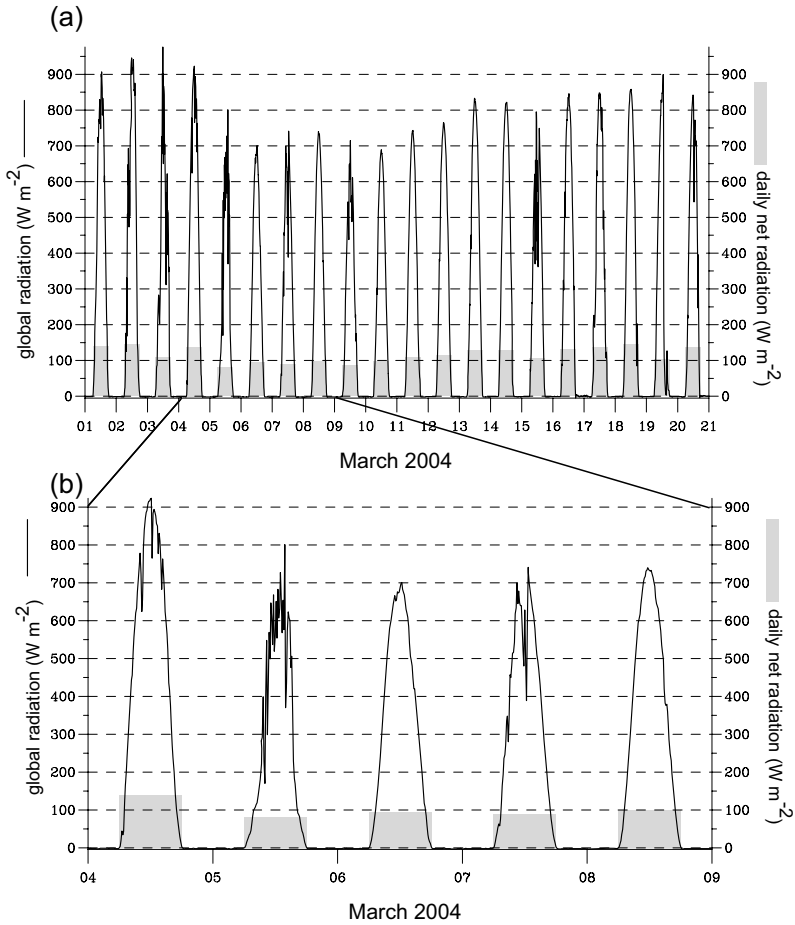


Figure 5. Ten minute total down-welling short-wave radiation (lines) and 24-hour (06–06 UTC) net full-spectrum radiation (grey bars) at Cotonou: (a) 1–21 March 2004 and (b) 4–9 March 2004.

of the extraordinary heat wave on the day before the dust front arrived: firstly, there was no cooling sea-breeze and, secondly, solar radiation at the ground was unusually strong because the formation of fair-weather cumulus was suppressed.

A drop in visibility from 8 to 0.6 km and in RH from >90 to 30%, accompanied by a shift in wind direction from SE to N–NE and a 24-hour pressure increase of 2–3 mb, indicate the passage of the dust front around 06 UTC 5 March (Fig. 6). Until 8 March, dry and hazy harmattan conditions continued with daily minimum RH values below 20% and even down to 16% on 5 March. On 9 March, surface humidity returned to near-normal values. Except from upper-level clouds on 5, 7 and 9 March, evident in the jagged global radiation curves on these days in Fig. 5(a), cloudless conditions prevailed until 15 March. However, the surface global radiation and the 24-hour net radiative forcing did not reach the large values observed before the dust event until 16 March (Fig. 5(a)). The low values of total down-welling short-wave radiation are probably related to high values of dust aerosol content in the surface layer above Cotonou. This led to net radiation values of around $130 W m^{-2}$ being reduced to less than $100 W m^{-2}$.

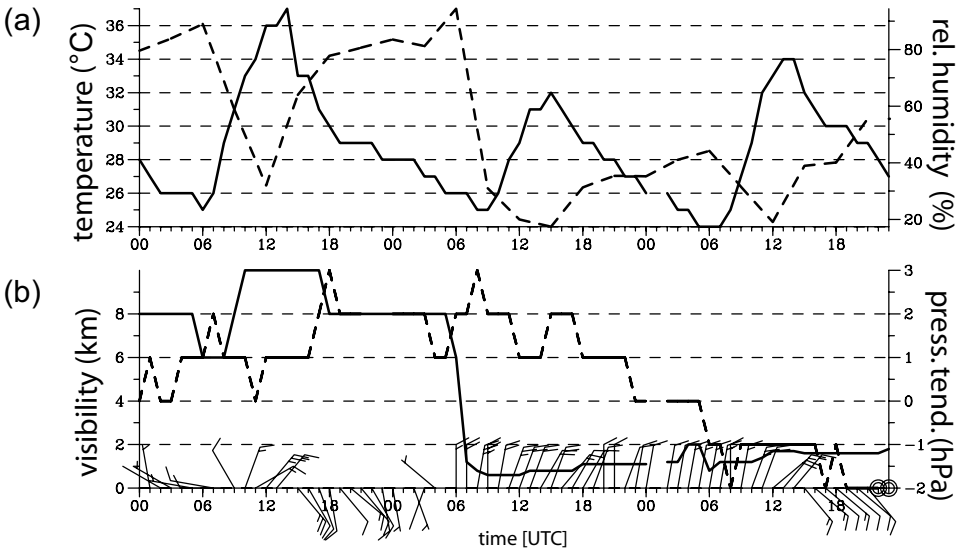


Figure 6. Observations at Cotonou between 00 UTC 4 March 2004 and 23 UTC 6 March 2004: (a) air temperature ($^{\circ}\text{C}$, solid line) from hourly METAR reports and relative humidity (%), dashed line) from 3-hourly SYNOP reports, and (b) as in (a) but for METAR 24-hour pressure tendency (hPa day^{-1} , dashed) and hourly visibility (km, solid). The hourly humidity observations from the METAR reports were not used because the measuring site was considered unrepresentative. Wind barbs as in Fig. 3: half barb = 5 knots, full barb = 10 knots, triangle = 50 knots.

Surface pressure at Cotonou and Parakou remained higher than before the dust event until 17 March (not shown).

These observations suggest that the intense and large-scale dust outbreak caused a considerable equatorward displacement of the ITCZ (compare Figs. 1(a) and 12(b) with Fig. 1(b)). The hazy air behind the front reduced the solar radiation reaching the ground substantially, which slowed down the return of the heat low over the continent. As a consequence, the ITCZ over the western Gulf of Guinea remained along the Ivory Coast at $4\text{--}5^{\circ}\text{N}$ for about two weeks, far south of its climatological position. National Oceanic and Atmospheric Administration (NOAA) outgoing long-wave radiation (OLR) data for the period in question indicate an axis of strongest convective activity, i.e. lowest OLR values, at the equator and positive OLR anomalies to the north exceeding 35 W m^{-2} over a wide area (not shown). This is associated with an anomalous dry March 2004 in the Soudano-Guinean zone with first March rainfalls at Cotonou falling on the 16th.

4. LARGE-SCALE FLOW FIELDS

(a) Upper-level PV

Following TF97 we will employ PV diagnostics to describe the large-scale evolution at upper levels leading up to the dust storm described above. Figure 7 shows PV, PV advection and wind on the 325 K isentropic surface (isopleths and vectors), together with diabatic PV tendencies in the 200–250 mb layer related to the change in vertical stability caused by latent-heat release (shading). The 325 K level is located in the lower stratosphere (200–250 mb) at midlatitudes and reaches down to about 500 mb in the tropics (see Fig. 9(a)). To facilitate a comparison with Fig. 8, the positions of surface lows and 925 mb anticyclonic centres are indicated (see subsection 4(b)).

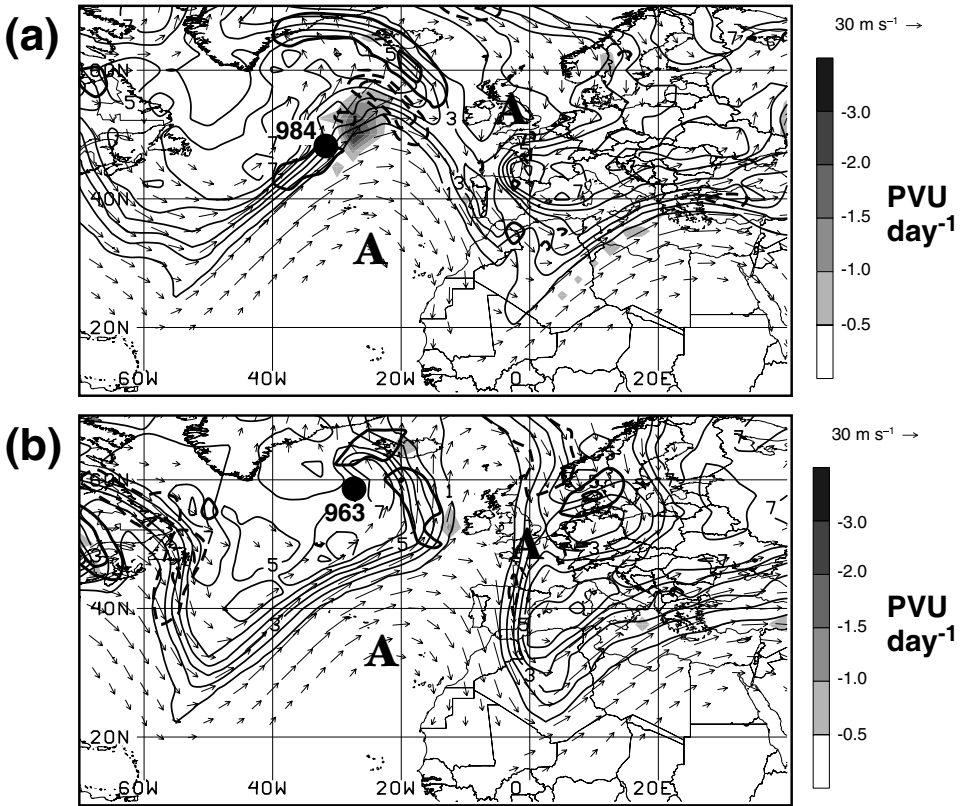


Figure 7. Potential vorticity (PV), PV advection and total wind on the 325 K potential-temperature surface, and diabatic PV-tendency in the 200–250 mb layer, at 12 UTC: (a) 1 March 2004 and (b) 2 March 2004. PV contours (thin lines) are at 1, 2, 3, 4, 6 and 8 PVU with the 4 PVU contour in bold. PV-advection contours are thick lines at intervals of 10^{-4} PVU s^{-1} . Total wind vectors are according to the scale in the upper-right corner; only winds greater than 15 m s^{-1} are plotted. The diabatic PV tendency in the 200–250 mb layer (PVU day^{-1}) is shaded following the grey scale. The positions (●) and central pressures (mb) of the surface cyclones and the positions (A) of the 925 mb anticyclones referred to in the text are indicated (cf. Fig. 8).

At 12 UTC 1 March 2004, about 26 hours before the beginning of the dust outbreak, strong gradients of PV over the central North Atlantic indicate a strong SW–NE oriented upper-level jet (Fig. 7(a)). In its left-exit region, is a surface cyclone with a central pressure of 984 mb. North-east of the centre are extreme negative diabatic PV tendencies as low as -3 PVU day^{-1} ($1 \text{ PVU} = 10^{-6} \text{ m}^2\text{K}^{-1}\text{s}^{-1}$) and pronounced negative PV advection. IR imagery shows a thick cloud-band in this region around that time (not shown). A marked PV ridge is located over the subtropical Atlantic and a PV trough stretches into north-west Africa, but at this time PV values below 4 PVU are confined to the Mediterranean region, consistent with a predominantly upper-level feature over Africa. Farther downstream, another strong jet and moderate PV tendencies are found to the north of Libya.

Over the next 12 hours the central pressure of the surface low fell explosively by 25 mb to 959 mb (not shown). This deepening rate lies above the 99 percentile of the climatology presented by Roebber (1984, his Fig. 1). Figure 7(a) suggests a crucial role for latent heat in the explosive deepening process, potentially in the fashion of a diabatic

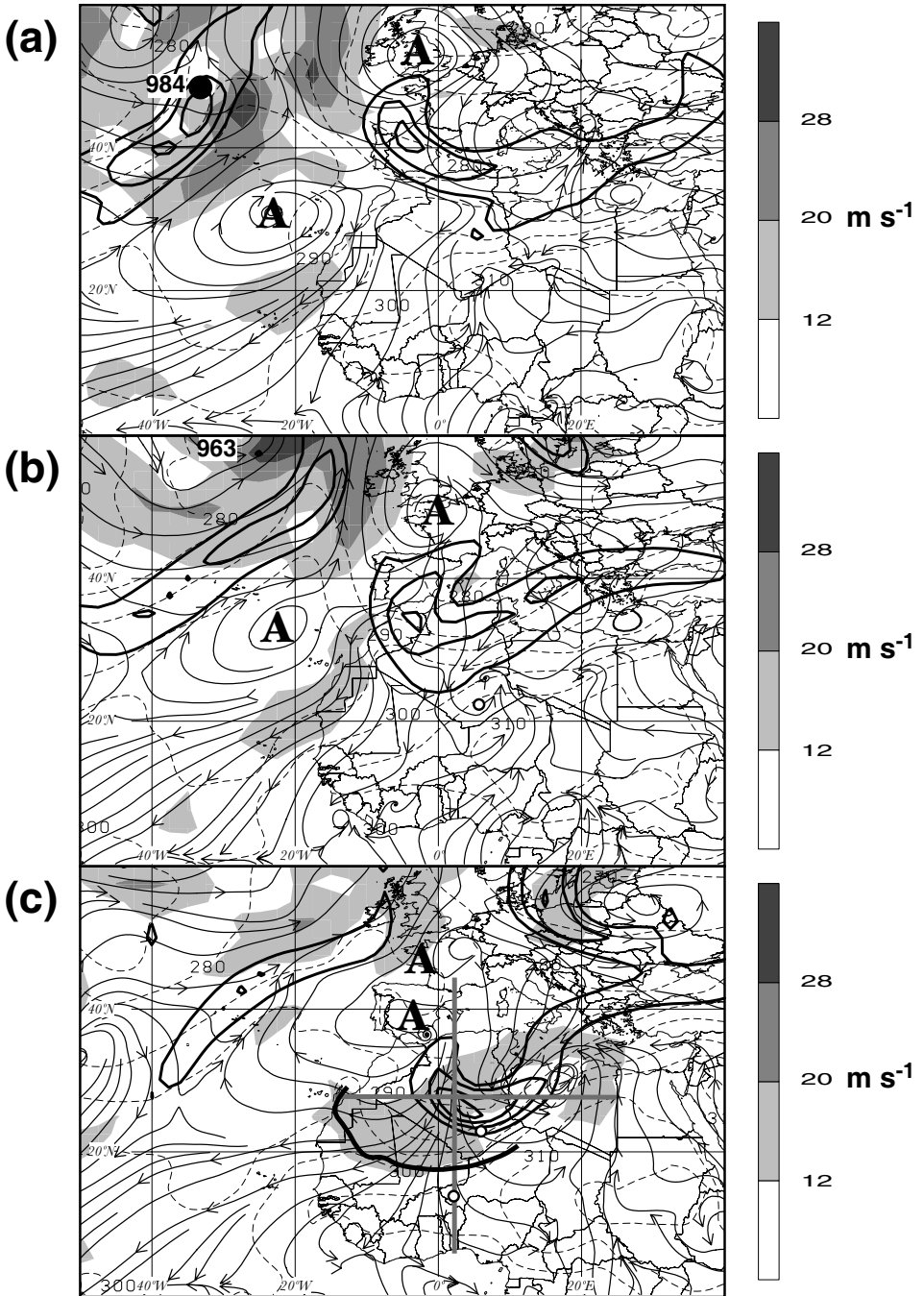


Figure 8. 925 mb streamlines, isentropes and wind speed at 12 UTC: (a) 1 March 2004; (b) 2 March 2004; (c) 3 March 2004 and (d) 4 March 2004. Isentropes (dashed) are at 5 K intervals. Wind speeds (at 8 m s^{-1} intervals) are shaded following the grey scale. The positions (●) and central pressures (mb) of the surface cyclones and the positions (A) of the anticyclonic circulation centres referred to in the text are indicated. The closed patterns of thick black lines indicate upper-frontal zones; they are isopleths of the gradient of the 700–400 mb thickness (at $10 \text{ gpm } [100 \text{ km}]^{-1}$ intervals, with values less than $20 \text{ gpm } [100 \text{ km}]^{-1}$ suppressed). The bold thick line in (c) and (d) marks the dust front identified in satellite imagery (cf. Fig. 3). Straight grey lines in (c) mark the position of the cross-sections shown in Fig. 9 and open circles in panels (b)–(d) the locations of the radiosonde stations Tamanrasset and Niamey, respectively (see Fig. 4).

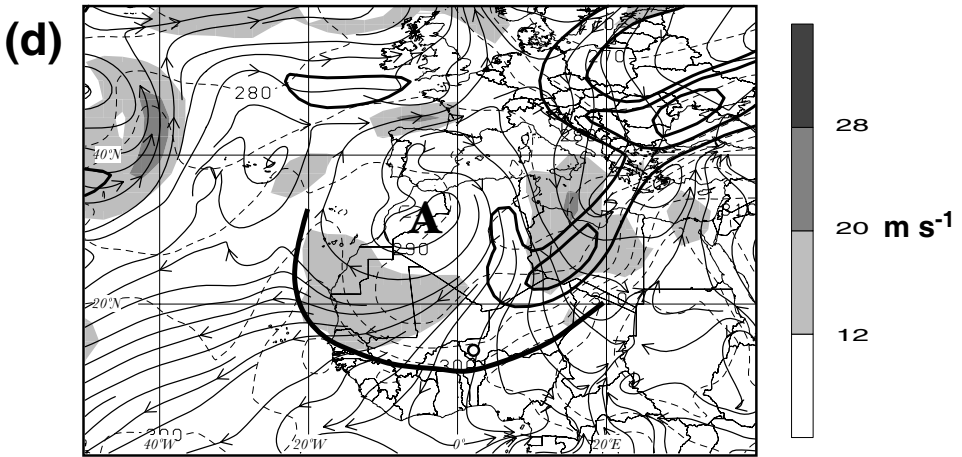


Figure 8. Continued.

Rossby wave (Wernli *et al.* 2002). By 12 UTC 2 March (Fig. 7(b)), the cyclone has moved northwards and started to fill. The PV ridge has dramatically amplified and now stretches into arctic latitudes. Diabatic PV tendencies have weakened and substantial negative PV advection is confined to the north-eastern flank of the amplified ridge. The amplification of the PV ridge causes a tightening of PV gradients and a southward advection of high-PV air over western Europe, resulting in an intensification of the PV trough over North Africa.

This analysis suggests that the massive diabatic PV destruction in connection with the extreme cyclogenesis over the North Atlantic, together with advection of low PV from the subtropics, significantly contributes to the wave amplification and the penetration of unusually high PV values to North Africa. The short temporal and spatial scale of the diabatic PV destruction probably helps the evolution, since it generates a very compact strong anomaly that is displaced far into high latitudes with the strong upper-level winds, before mixing can dilute it. Knippertz and Martin (2005) found similar large-scale evolutions upstream of low-latitude troughs affecting West Africa.

About 2 hours after the 12 UTC analysis shown in Fig. 7(b), the dust front formed near the southernmost extension of the 4-PVU contour over Algeria (see subsection 3(a)). The position of the dust storm to the south and a little to the west of an upper-level trough (positive PV anomaly) is as analysed by Kalu (1979) and TF97.

(b) Low-level flow

Figure 8 shows streamlines, isentropes (dashed) and wind speed (shading) at 925 mb for 12 UTC 1–4 March. In addition, the magnitude of the gradient of the 700–400 mb thickness is plotted to indicate frontal zones in the mid- and upper-troposphere. At 12 UTC 1 March, a large subtropical anticyclonic circulation (A) lies beneath the upper-level PV ridge over the eastern subtropical Atlantic (Figs. 7(a) and 8(a)). Over West Africa, the streamlines indicate moderate cold advection. Another closed anticyclonic system lies over the British Isles, east of the thermal ridge over the North Atlantic. This feature has a weaker PV signal at 325 K (Fig. 7(a)). Corresponding to the upper-level PV field (Fig. 7(a)), there is a sharp upper front over the Iberian Peninsula. It is associated with moderate gradients in 925 mb potential temperature θ

over north-west Africa (Fig. 8(a)). The explosively deepening surface cyclone of 984 mb (see subsection 4(a)) is connected to a distinct upper-front and extraordinary low-level wind speeds of more than 30 m s^{-1} .

By 12 UTC 2 March, the intensification and northward movement of the cyclone has pushed the warm air over the North Atlantic further north accompanied by strong low-level winds and a weakening upper-front (Fig. 8(b)). During this period, the centres of the two anticyclones are almost stationary, but the streamlines indicate the beginning of a merging of the two systems, consistent with the amplification of the upper PV ridge (Fig. 7(b)). Further downstream, the upper-front has moved southward into north-west Africa, where low-level θ -gradients are tightening. The rainfalls over Algeria described in subsection 3(a) are associated with this cold front.

During the next 24 hours, the two low-level anticyclones continue to approach each other (Fig. 8(c)). While that over Iberia is associated with distinct northerly cold advection over North Africa, that over France feeds cold air into the circulation of the cyclone that has developed over Libya. The former flow reveals similarities to trade surges in connection with upper troughs to the west of West Africa (Knippertz and Martin 2005). By this time, the intensified upper-front is over central Algeria. The low-level θ -front has started to detach itself from the upper-feature and has moved to the south-west, consistent with the change in temperature profile between 2 and 3 March at Tamanrasset (Fig. 4(a)). The reasons for this behaviour of the low-level front will be discussed in subsection 5(b). The dust front (thick black line in Fig. 8(c), see also Fig. 3(d)) is located at the leading edge of the southward penetrating cold air in agreement with the station observations summarized in subsection 3(a). The strong low-level winds help to transport dust to the south and to mobilize more dust farther north.

By 12 UTC 4 March, the subtropical anticyclone has intensified with wind speeds greater than 12 m s^{-1} south of the centre (Fig. 8(d)). The low-level cyclone has moved from Libya to the Mediterranean Sea and has a strong northerly flow on its western flank. The release of latent heat associated with the intense precipitation over Algeria and Libya (see subsection 3(a)) has warmed the mid-level cold pool, thereby weakening the thickness contrast along its southern side (Fig. 8(d)). The low-level cold air and the dust front along its leading edge have continued to move away from the upper-front and have penetrated into the Sahel (cf. Fig. 4(b)), while over the subtropical Atlantic Ocean dust-laden air flows northwards around the anticyclone (cf. Fig. 1(a)). The breakdown of the monsoon southerlies on 4 March described in subsection 3(c) may be seen by comparing streamlines drawn over tropical West Africa on 1 and 4 March (Figs. 8(a, d)).

(c) *Cross-sections*

Figure 9(a) shows a meridional cross-section along 2.5°E that cuts through the northerly flow to the west of the axis of the upper-level trough (grey line in Fig. 8(c)). The position of the dust front is shown by the thick grey bar beneath Fig. 9(a). It lies in the southern part of a region with a marked horizontal temperature gradient at the surface (15 K between 15.5° and 21.5°N), strong cold advection and almost vertical isentropes below 850 mb. The 12 UTC 3 March radiosonde ascents at Tamanrasset (Niamey) in Fig. 4 were taken just to the north-east (south) of this region (open circles in Fig. 8(c)). The coldest surface air ($\theta < 285 \text{ K}$) is around 28°N over Algeria. Somewhat warmer air in the lee of the Atlas mountain chain is probably related to a föhn wind (cf. Fig. 8(c)). The highest surface-temperatures occur near the border between Benin and Niger, a typical location of the heat low at that time of the year (cf. subsection 3(c)). In the tropics, winds in the lowest layers are northerly all the way south to 10°N .

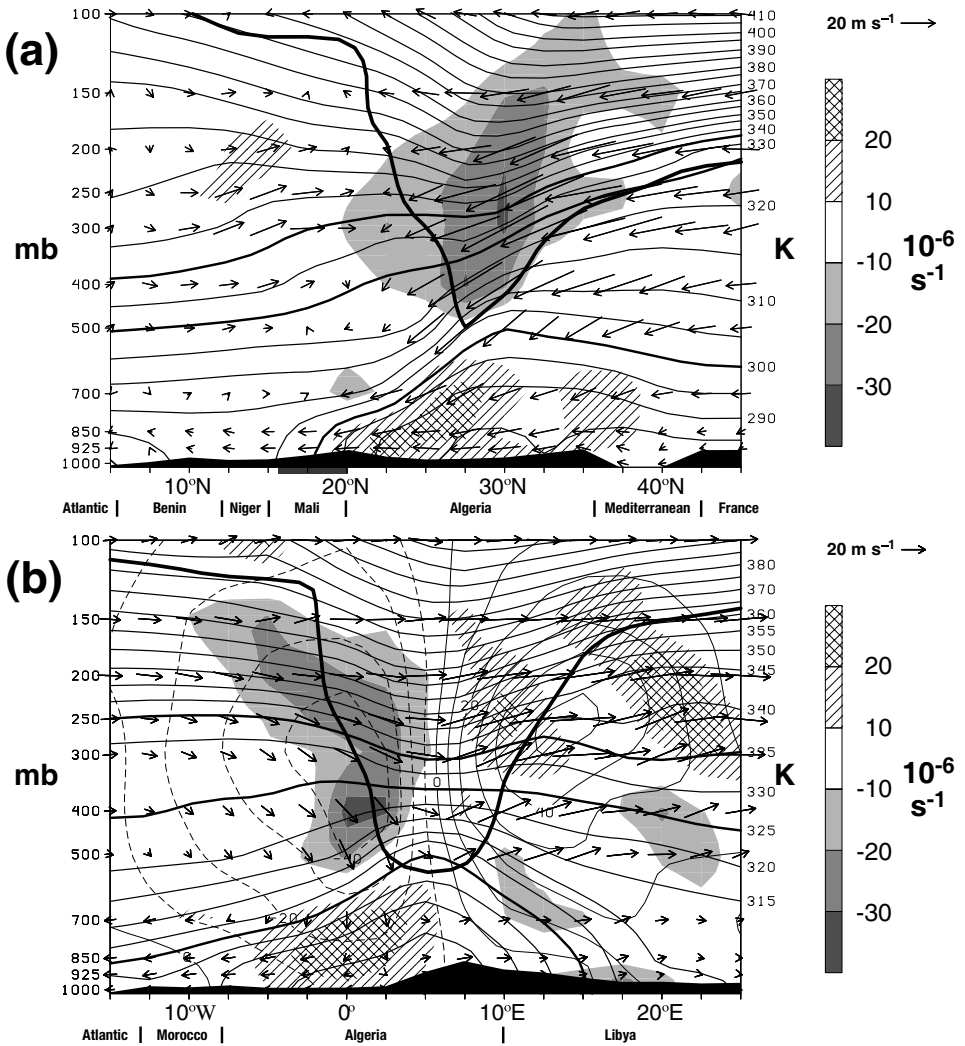


Figure 9. Cross-sections for 12 UTC 3 March 2004 (see Fig. 8(c)): (a) meridional cross-section along 2.5°E and (b) zonal cross-section along 27.5°N . In both panels: vertical and horizontal winds in the plane of the section are combined into single vectors, using the linear scale in the top-right corner for the horizontal wind and a logarithmic scale for the vertical component with maximum descending motion of $+10 \mu\text{b s}^{-1}$; isotherms of potential temperature are at 5 K intervals with 300 K, 325 K and 335 K shown in bold; the 2 PVU isopleth is shown as a heavy black line; values of divergence (10^{-6} s^{-1}) use the scale on the right-hand side; at the bottom of each panel, the ECMWF model orography in the plane of the section is shown in black. Beneath panel (a), the region of the dust front is indicated by a thick dark grey bar, between about 16°N and 20°N (cf. Fig. 3(d)). In panel (b), thin dashed lines are isotachs of northerly wind (out of the page) and thin continuous lines southerly wind (into the page) at intervals of 10 m s^{-1} .

Near 30°N over Algeria, a region of very strong northerly winds at all levels accompanies upper-level (450–150 mb) convergence, mid-level subsidence and divergence below 600 mb. The strong subsidence at mid- and upper-levels leads to a conspicuous lowering of the dynamical tropopause defined by the 2 PVU isopleth (bold black line in Fig. 9(a)), bringing stratospheric air down to below 500 mb. The arching of the isentropes below the positive upper-PV anomaly is typical of cold-core structures (cf. TF97, Fig. 13(a); Hoskins *et al.* 1985, Fig. 8). The detachment of the low-level cold air from

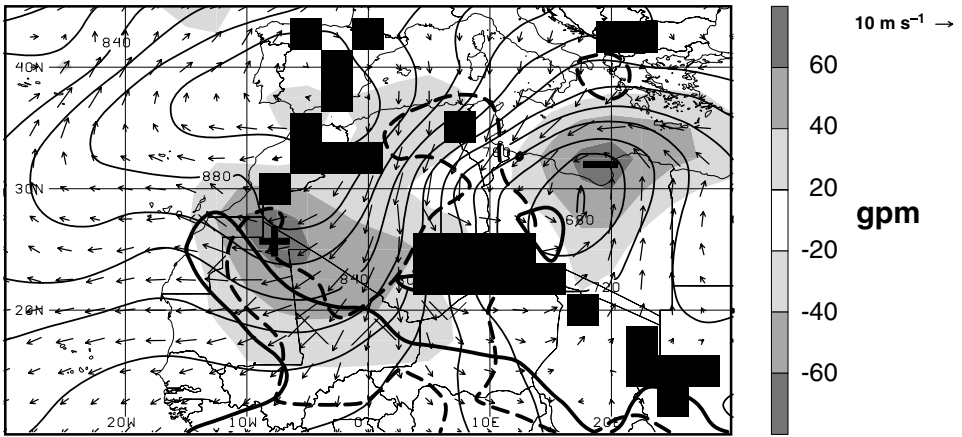


Figure 10. Flow at 925 mb 12 UTC 3 March 2004: geopotential height (thin lines, 20 gpm intervals), 12 hour tendency of geopotential height (00–12 UTC) (gpm per 12 hours, according to legend; + marks the area of maximum rise in height of the 925 mb surface and – the area of greatest fall); wind (vectors according to scale in upper-right corner); regions with isallobaric {ageostrophic} wind greater than 4 m s⁻¹ {8 m s⁻¹} (border shown by thick solid {dashed} lines); region of thick dust (hatching) (from Fig. 3(d)). Black boxes denote areas where the 925 mb surface is below the ECMWF model topography.

the upper front associated with the low tropopause is evident from this cross-section (Fig. 9(a)), if, for example, one follows the 300 K isentrope. The strong subsidence is consistent with the warming and drying above the cool and dusty surface layer evident in the sounding from Tamanrasset for 12 UTC 3 March (Fig. 4(a)).

A zonal cross-section along the latitude of the lowest tropopause in Fig. 9(a), i.e. 27.5°N (grey line in Fig. 8(c)), shows an even more pronounced cold dome over Algeria and a flow of cold air down the north-westernmost slope of the Hoggar (in the smoothed ECMWF-model orography). This is, again, accompanied by strong upper-level convergence, subsidence and low-level divergence. Figure 9(b) will be further discussed in subsection 5(a).

(d) Isallobaric-wind analysis

Figure 10 shows 925 mb geopotential heights z and winds at 12 UTC 3 March 2004. Consistent with the rise in surface pressure over the western Sahara (Fig. 3) and the intensifying anticyclonic circulation at 925 mb (Fig. 8), z increases by more than 60 gpm between 00 and 12 UTC (shading in Fig. 10), leading to a substantial southward extension of the anticyclone over Iberia into North Africa. The horizontal gradient of the geopotential height tendencies on a pressure surface is related to the isallobaric wind through

$$\mathbf{v}_{\text{is}} = -\frac{g}{f^2} \cdot \nabla_p \left(\frac{\Delta z}{\Delta t} \right),$$

where g is the gravitational acceleration and f is the Coriolis parameter. Given its dependence on f^{-2} and the rapid decrease of f towards low latitudes, \mathbf{v}_{is} reaches values of more than 4 m s⁻¹ along the southern flank of the anticyclone (thick solid line in Fig. 10). Here \mathbf{v}_{is} accounts for about half the strong ageostrophic wind (thick dashed line) and considerable parts of the total wind. This demonstrates that the surge-like southward displacement of the dust during this phase is, to a great extent, driven by the rapid anticyclonogenesis.

At the same time, strong negative height-tendencies over the Gulf of Sirte (see Fig. 2), where hot Saharan air is advected northward ahead of the upper-level trough (Fig. 8(c)), cause the formation of a low-level cyclone over central Libya (Fig. 10). The enhanced pressure gradient between the low and the anticyclone to the west produces a north-easterly flow that feeds moist Mediterranean air into the precipitation zone described in subsection 3(a) and strong northerly winds over Algeria that cause the dust mobilization behind the leading dust front (see Fig. 3(d)). Considerable isallobaric winds are deduced to the south-west of the low. Apart from the regions of strong isallobaric winds, Fig. 10 shows large ageostrophic winds in the region of the Atlas Mountains in northern Algeria and the Hoggar in south-eastern Algeria, which are most likely related to surface friction.

5. DYNAMICS

(a) *Balanced versus unbalanced dynamics*

The observational analysis in the previous section shows us that two large-scale factors were of crucial importance in the generation and the sustenance of the dust storm. Firstly, the amplification of the tropopause-level PV wave over the North Atlantic caused the penetration of a cold front and an upper PV-trough into North Africa and that this was associated with strong surface winds over the Sahara. Secondly, the strong pressure gradients and isallobaric winds resulting from explosive anticyclogenesis (cyclogenesis) upstream (downstream) of the trough supported further dust mobilization and a quick displacement to the south and west.

Figures 7, 8 and 10 show that the low-level anticyclogenesis occurred in a region of strong northerly flow associated with cold advection and negative vorticity advection (NVA) as a result of the β -effect. This indicates a large quasi-geostrophic (QG) contribution to subsidence and to positive height-tendencies. QG theory is a dynamical concept for balanced flows and is a good approximation for synoptic scale forcing in most midlatitude weather systems. In the present case, however, the explosive evolution and significant ageostrophic wind components (Fig. 10) suggest substantial contributions from other (unbalanced) dynamic processes. Figure 9(b) supports this hypothesis: despite the rather symmetrical upper PV-anomaly, there is a large asymmetry in the fields of divergence and vertical motion. In addition, while northerly winds of up to 16 m s^{-1} reach the surface to the west of the PV anomaly (near 2.5°E ; see also Figs. 3(d), 9(a) and 10), southerly winds farther east are considerably weaker (thin isopleths in Fig. 9(b)). According to Hoskins *et al.* (1985), the depth to which a PV anomaly will induce winds is determined by fL/N , where L is the horizontal length scale of the PV anomaly and N the Brunt–Väisälä frequency. For 27.5°N , 5°E and the layer between 925 and 500 mb N is 0.0114 s^{-1} . Taking L to be 8 degrees of latitude (889 km), we obtain a penetration depth of 5.2 km, which, see Fig. 9, is roughly the vertical distance between the ground and the 2-PVU contour at its lowest point. This demonstrates that the low altitude of the PV anomaly is a crucial precondition for the existence of strong winds at lower levels (cf. Fig. 13 in TF97). The Brunt–Väisälä frequency* increases to the west of the PV anomaly, as do the near-surface winds. This suggests a substantial inconsistency between the low-level flow and the upper-level PV field.

In order to quantify the part of the mass field resulting from such unbalanced processes inconsistent with the PV distribution, we performed a PV inversion. Hoskins *et al.* (1985) showed that, given, firstly, a balance condition relating the mass and momentum

* The Brunt–Väisälä frequency is related to the vertical gradient of potential temperature, which is plotted in Fig. 9(b).

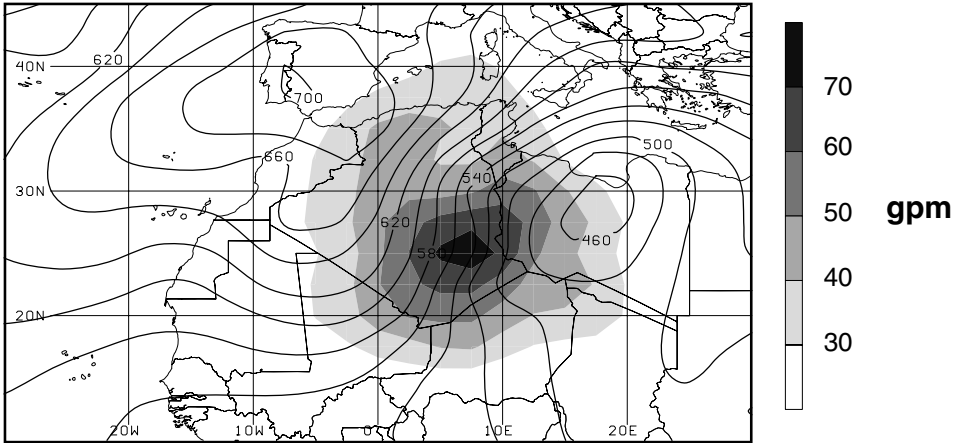


Figure 11. Geopotential height at 950 mb for 12 UTC 3 March 2004 (contours at 20 gpm intervals). Shading shows the difference between analysed heights and heights found through PV inversion ($z - z_{PI}$) (gpm, using the grey scale). For more details, see text.

fields and, secondly, suitable boundary conditions on a given domain, knowledge of the PV distribution is sufficient to recover the full kinematic and thermodynamic structure of the atmosphere within that domain. This property of PV is usually referred to as invertibility. Davis and Emanuel (1991) developed a PV inversion scheme, based upon the fairly high-order Charney nonlinear balance, which yields an excellent approximation to observed flows (Davis *et al.* 1996). Here we use vertically interpolated PV values every 50 mb between 900 and 100 mb and θ at 925 and 75 mb (linearly interpolated between 950 and 900 mb, and 100 and 50 mb, respectively) as boundary conditions for the PV inversion on a domain spanning 5°N – 60°N , 32.5°W – 32.5°E . A lower boundary condition of 925 mb was preferred to 975 mb because of the high terrain over North Africa (see Figs. 2 and 10). This should make a difference only when the lowest kilometre of air is extremely stable, which is untypical of the low latitudes we are dealing with here. Negative values of PV are set to 0.001 PVU. From the inversion we retain fields of geopotential height (termed z_{PI}) and non-divergent stream-function consistent with the nonlinear balance condition. A similar computational approach has been used in a study by Martin and Otkin (2004).

By subtracting z_{PI} from the analysed z we obtain the portion of the mass field that is related to processes not incorporated in the nonlinear balance condition. This allows an evaluation of their importance for the geopotential-height tendencies shown in Fig. 10. Figure 11 shows contours of geopotential height and fields of the difference $z - z_{PI}$ (shaded) at the lowest level used for the PV inversion (950 mb). At 12 UTC 3 March, when the dust front was spreading quickly south- and west-ward (Fig. 3(d)), an imbalanced height of +77 gpm is found in the region of strongest west–east z gradients over south-eastern Algeria. Being of the same magnitude as the 12-hour height tendencies shown in Fig. 10, this value implies that the explosive south-eastward extension of the low-level anticyclone is largely produced by imbalanced dynamics. On the other hand, the cyclogenesis over Libya also occurs in a region of fairly large positive $z - z_{PI}$. This indicates that unbalanced processes suppress a deepening of the low, even though the position of the distinct mid-level PV-anomaly with respect to the low-level baroclinic zone to the east of the Hoggar (Fig. 9(b)) seems favourable for cyclogenesis (TF97). This may explain why, despite 500 mb geopotential heights as low as 5640 gpm,

relative vorticity values up to $2.1 \times 10^{-4} \text{ s}^{-1}$ (more than three times f), geostrophic winds of more than 100 m s^{-1} and an ageostrophic component 1.5 times larger than the actual wind (not shown), a clear surface pressure minimum is not observed before 00 UTC 4 March 2004. The QG forcing for uplift associated with the massive advection of positive vorticity to the east of the trough axis and the low vertical stability (500 mb temperatures down to -25°C) together, however, support the occurrence of extreme precipitation in Libya (subsection 3(a)). In the following two subsections we shall discuss processes that contribute to the generation of the unbalanced mass maximum. These include evaporational cooling (subsection 5(b)), latent heating, inertial instability and friction (subsection 5(c)).

(b) *Evaporational cooling and the development of a density current*

In subsection 3(a) we have shown that unusually cold air near the surface accompanied the dust outbreak across the Sahara. Daytime temperatures of about 5°C in Algeria on both 2 and 3 March (Figs. 3(a) and (d)) required strong compensation for the effects of the föhn wind in the lee of the Sahara Atlas Mountains and for the advection of air from the Gulf of Gabès (Fig. 3(e)) where surface water temperatures were about 16°C . A dramatic dew-point increase (e.g. at AD), together with, at best, light precipitation at most stations in the northern Sahara, indicates substantial evaporational cooling of the cold frontal precipitation in the deep and dry Saharan planetary boundary layer (PBL) at midday on 2 March. Eventually, the föhn winds enhanced the dryness even further (see the cloud-free region in the lee of the Atlas chain in Fig. 3(b)). The evaporation of rain near the surface is supported by a Tropical Rainfall Measuring Mission (TRMM) Precipitation Radar overpass at 08 UTC (not shown). At that time, rainfall intensities were still relatively weak, but several areas of precipitation not reaching the ground can be identified. To get a rough idea of how much rain is needed to generate the observed cooling, we calculated the mass of water that has to evaporate per m^2 to lower the temperature in the lowest 200 mb of the atmosphere by 11 K. Using $m_1 = (\Delta T \cdot m_d \cdot c_{pd})/L$ with m_1/m_d being the mass of water/dry air per m^2 , ΔT the temperature change, c_{pd} the specific heat of dry air at constant pressure and L the latent heat, we obtain a value for m_1 of 9 kg m^{-2} , i.e. 9 mm of evaporating rain.

In addition, the abrupt pressure increase accompanying the passage of the dust front in its initial stage and its evolution in satellite imagery (Fig. 3) are reminiscent of a horizontally spreading, surface density-current fed by evaporationally cooled sinking air. From Figs. 3(a)–(c), we estimate a propagation speed of the dust front of approximately 16 m s^{-1} between 18 UTC 2 March and 06 UTC 3 March 2004. This is the period when the dust front became detached from the actual cold front over North Africa and formed a shallow layer of cold surface air with a steep leading edge as revealed by Figs. 4 and 9(a). Several studies have compared observed propagation speeds of cold fronts to the speed of a theoretical density current that varies with the square root of the density difference between the two uniform fluids involved (Benjamin 1968). However, as pointed out by Smith and Reeder (1988), in the real atmosphere the large uncertainty in determining the density difference and the height of the density current, together with the weak dependence of the propagation speed on these variables, impede a meaningful comparison between observed and theoretical velocities.

According to Smith and Reeder (1988), a more robust test is the existence of positive relative feeder flow behind the front, i.e. a region where the wind speed is greater than that of the leading edge of the cold air. Using the propagation speed of 16 m s^{-1} at 00 UTC 3 March and a meridional cross-section along 2.5°E (as in Fig. 9(a)) we indeed find a small region over Algeria, where the relative flow at

925 mb is southward (and downward, not shown). Another important precondition for the formation of a density current is a neutral stratification in the less dense fluid (Smith and Reeder 1988). The sounding at Tamanrasset ahead of the dust front shows that this condition was fulfilled in the typically adiabatic Saharan PBL up to about 700 mb (Fig. 4(a)). Other typical characteristics of density currents like the hydraulic head and the elevated nose cannot be identified in the coarse resolution ECMWF analysis data, but at least the former is evident in VIS satellite images around sunset on 3 March (not shown). Most probably, the orography of the Atlas Mountains and the Hoggar contributed to an acceleration of the density current to the south and west (see Fig. 9).

At later stages (Figs. 3(d)–(e)), the propagation speed of the dust front decreased, consistent with the decreasing depth of the density current (Fig. 4; Benjamin 1968). At that time, the synoptic-scale wind-field associated with the anticyclogenesis over north-west Africa appears to determine the propagation of the dust plume (see subsection 4(b)).

The previous analysis shows that a substantial part of the unbalanced dynamics (see subsection 5(a)) is related to the existence of the density current; other contributing factors will be discussed below. Several earlier studies have documented dust mobilization in connection with strong low-level winds and cold outbreaks (e.g. Kalu 1979; TF97), but density currents were not discussed explicitly. However, the extraordinarily low temperatures observed by TF97 (their Figs. 6 and 7) and several precipitation observations from central Algeria not mentioned in TF97 suggest a similar mechanism, which deserves further study.

(c) *Further unbalanced processes*

For a further analysis of the causes of the extreme anticyclogenesis over North Africa, we will now focus on the associated strong upper-level convergence and mid-level subsidence evident from Fig. 9. For 12 UTC 3 March, Fig. 12(a) shows the divergent part of the wind field and isotachs of the total wind at the 335 K level, where convergence reaches a maximum in Fig. 9(a). In this quasi-horizontal view, there is a pronounced convergence maximum over central Algeria. The northerly divergent winds from south-western Europe indicate contributions to the convergence maximum from balanced QG dynamics (see subsection 5(a)). We will now discuss contributions from unbalanced processes not covered in subsection 5(b).

Dashed isopleths in Fig. 12(a) mark regions of negative absolute geostrophic vorticity in the entrance region of the strong subtropical jet (STJ) that reaches wind speeds of up to 77 m s^{-1} to the east of the trough over Africa. This indicates inertial instability, which is associated with divergent cross-jet acceleration and an enhancement of convergence and subsidence farther downstream (Fig. 12(a)). The IR image in Fig. 12(b) shows that the continuous cloud-band along the equatorward flank of the STJ (also evident in Fig. 3(d)) is connected to convection over tropical Africa and therefore fulfils the definition of a tropical plume (TP) or moisture burst given by McGuirk *et al.* (1987). This result is consistent with a TP study by Knippertz (2005) who showed that buoyancy-driven subgeostrophic parcels from low latitudes accelerate into the STJ as a result of a strong pressure-gradient between an extratropical trough and northern tropical latitudes. At low latitudes, where f is small, this pressure-gradient force cannot be balanced fast enough and the flow becomes inertially unstable. The streamlines in Fig. 12(b) do indeed indicate an inflow of near-equatorial air into the STJ. The meridional cross-section in Fig. 9(a) reveals upper-level divergence, ascent and southerly flow near the base of the TP over Niger. The latter converges with the extratropical flow in the subtropics.

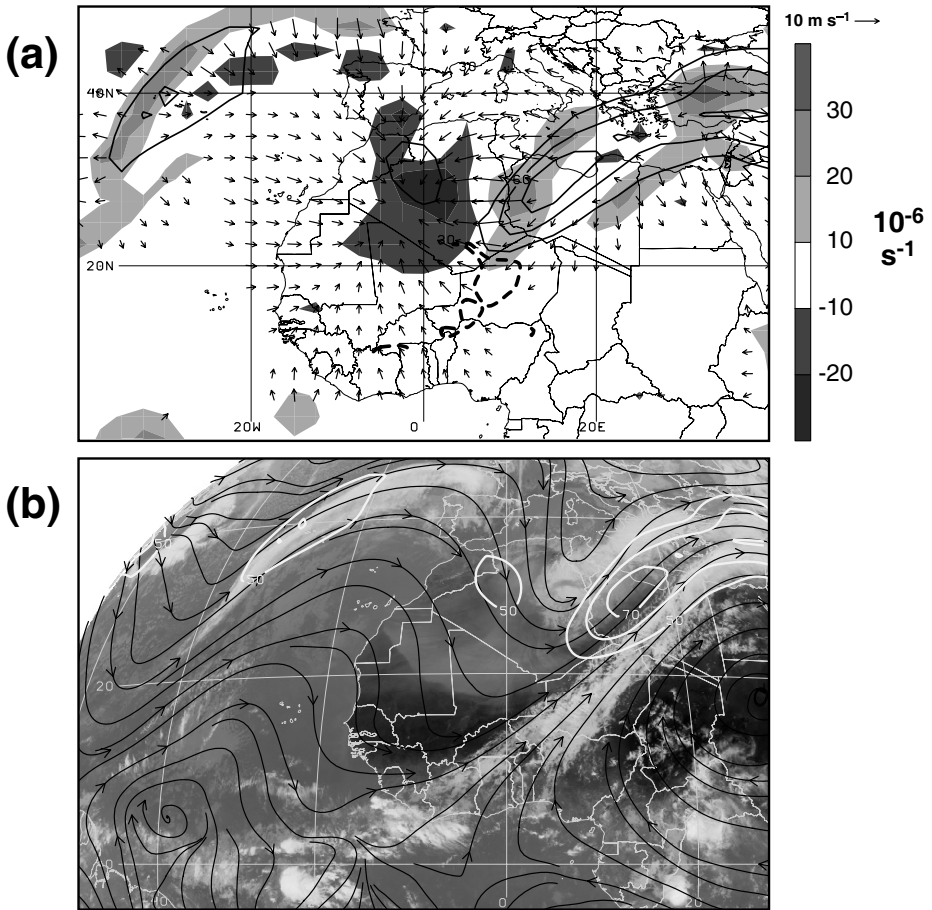


Figure 12. Potential temperature surface for 335 K, 12 UTC 3 March 2004. Isotachs of total wind (intervals 10 m s^{-1} , with values below 50 m s^{-1} suppressed), with: (a) divergent wind (vectors using length scale in top right corner); divergence (10^{-6} s^{-1} , using grey scale) and regions of negative absolute geostrophic vorticity (black dashed lines over Niger); (b) streamlines superimposed on Meteosat 7 IR satellite image.

The divergence maxima over Libya and the Mediterranean Sea in Fig. 12(a) are concomitant with dense cyclonically rotating clouds (Fig. 12(b)) and are related to the divergent outflow from the extreme precipitation over Algeria and Libya (see subsection 3(a)) that further contributes to the pumping of mass into the anticyclone to the west. The location of these rainfalls with respect to the TP is similar to events in Tenerife (Fink and Knippertz 2003) and Los Angeles (Knippertz and Martin 2006). Even though certainly an unbalanced process, surface friction will always counteract (anti-) cyclogenesis and is therefore an unlikely contributor to the maximum in $z - z_{PI}$ in Fig. 11.

It is noteworthy that two days earlier, at 12 UTC 1 March, a larger and denser TP with an even strong STJ of 87 m s^{-1} and pronounced inertial instability as far north as 24°N lay east of the trough over western North Africa (see Fig. 7(a)). Over central Algeria, there are large values of $z - z_{PI}$, although they are only half as great as those two days later on 3 March (Fig. 11). It seems likely that contributions from the pronounced inertial instability could not compensate for the absence of other substantial

non-balanced processes at this time, even though parts of the divergence along the jet axis may have been related to latent-heat release within the TP as indicated by Fig. 7(a).

This analysis suggests that the superposition of different unbalanced processes acting on the meso- and synoptic-scale in the course of 2–4 March was responsible for the extension, strength and persistence of the dust event. The relationship of TPs over Africa to Saharan dust storms has not previously been discussed in the literature, even though a TP is evident in Fig. 12 of TF97. Inertial instability and extreme subsidence have been described in various other TP studies (Mecikalski and Tripoli 1998; Knippertz 2005; Knippertz and Martin 2005), but not the related imbalance in the low-level height field.

6. CONCLUSIONS

We have investigated the synoptic evolution and the dynamics of a major dust outbreak over the Sahara in March 2004 on the basis of station observations, satellite images and ECMWF analysis data. The event was accompanied by very unusual weather including cold, windy and dusty conditions in large parts of northwest Africa, considerable rainfalls in the arid parts of Algeria and Libya, and maximum temperature records along the Guinea Coast. The outbreak culminated in a dust plume reaching from Morocco around West Africa into the Gulf of Guinea associated with a substantial and sustained southward push of the ITCZ. The analysis of this event unveiled some fairly new dynamical aspects of the generation of major Saharan dust outbreaks and harmattan surges. The most important findings are the following.

- The large-scale flow during this event was characterized by a high-amplitude upper-level wave with strong SW–NE oriented jets to the east of the troughs over the North Atlantic and North Africa. Strong latent heating occurred in a conspicuous cloud-band associated with an extreme cyclogenesis in the exit region of the former jet, causing a substantial diabatic destruction of upper-level PV. Together with the advection of low-PV air associated with the baroclinic development, this PV destruction led to a substantial amplification of the PV ridge over the North Atlantic and finally of the trough over North Africa.

- The intensification of the upper-level trough led to a penetration of a precipitating cold front from the Mediterranean Sea into Algeria. A mesoscale density-current-like flow associated with strong evaporational cooling in the dry desert air caused the initial dust-front. Orographic föhn effects supported this process. The dusty cool air quickly moved away from the upper cold frontal zone and formed an increasingly shallow layer on its way to the south and west, topped by adiabatically warmed air.

- Large advection of positive vorticity and warm air ahead of the intense PV trough triggered cyclogenesis and strong low-level winds. The incorporation of moist air from the Mediterranean Sea and the strong QG forcing for uplift produced extreme precipitation in the Libyan Desert. There was no prior cyclogenesis in the lee of the Atlas Mountains as reported by TF97. The extremely low tropopause associated with the PV anomaly agrees with observations of stratospheric intrusion during dust storms (Danielsen 1975; Alpert and Ganor 1993).

- The south- and west-ward synoptic-scale advection and lateral spreading of the dust front was related to strong isallobaric winds caused by pronounced upper-level convergence, sinking and anticyclogenesis over north-western Africa as in the pressure surge observed by Kalu (1979) (see also TF97). The subsidence forced the penetration of high-momentum, northerly, mid-level flow into the Saharan PBL that led to further dust mobilization.

- With respect to the dynamics of the anticyclogenesis, results from a PV inversion suggest that the effects of the cold advection and negative vorticity advection related to the upper-wave were substantially enhanced by contributions from processes incompatible with the assumption of a nonlinear balance. Besides the effects of the unusually heavy precipitation over North Africa (evaporational cooling and divergent outflow), inertial instability appears to have been of importance. This inertial instability was related to the acceleration of tropical air into the STJ east of the upper-trough and was associated with the formation of a TP. Extending the present work by using a numerical model to study the effects of individual unbalanced processes seems likely to produce interesting results.

- Towards the end of the dust outbreak, strongly subsided dry air ahead of the actual dust front reached the Guinea Coast, where it suppressed shallow convection. The concomitant, unusually large, pressure-rise in the near-equatorial tropics pushes the heat low over the equatorial Gulf of Guinea causing a breakdown of the monsoon south-westerlies along the Guinea Coast. The increased short-wave radiative forcing and the absence of cooling onshore winds resulted in a record heat-wave on the day before the dust front arrived. The ongoing high dust-concentrations in the tropical atmosphere after this event were associated with a slow recovery of the heat-low circulation and a retracted ITCZ. This suggests that, at least in some years, springtime Saharan dust outbreaks may play a crucial role in delaying the northward progression of the African monsoon. These effects should, therefore, if it is to succeed, be included in any model of this system.

ACKNOWLEDGEMENTS

The work presented here was accomplished during a two-year postdoctoral research scholarship for PK from the German Science Foundation (DFG; Grant KN 581/1–1) at the Department of Atmospheric & Oceanic Sciences of the University of Wisconsin–Madison under the supervision of Prof. Jonathan E. Martin and Prof. emer. Stefan L. Hastenrath. Support for AHF came from the interdisciplinary project IMPETUS funded by the German Ministry of Education and Research (BMBF) under grant 01 LW 0301A and by the Ministry of Science and Research (MWF) of the federal state of North Rhine-Westphalia under grant 223-21200200. We would like to thank Jonathan Martin, Michael Morgan, Jason Otkin and Francis Bretherton for fruitful discussions concerning the PV inversion and Volker Ermert for his assistance in producing Figs. 2, 4, 5 and 6. We are grateful to the National Services of Benin and Niger for providing us with data from their synoptic networks and to Chris Thorncroft for furnishing the METAR data. Helpful comments from two anonymous reviewers contributed to improve an earlier version of the manuscript.

REFERENCES

- | | | |
|-------------------------------|------|--|
| Alpert, P. and Ganor, E. | 1993 | A jet stream associated heavy dust storm in the western Mediterranean. <i>J. Geophys. Res.</i> , 98 , 7339–7349 |
| Benjamin, B. T. | 1968 | Gravity current and related phenomena. <i>J. Fluid. Mech.</i> , 31 , 209–248 |
| Cana, L. | 2002 | The Saharan dust episode of 26 February 2000 over the Canary archipelago: A synoptic overview. <i>Weather</i> , 57 , 385–389 |
| Chiappello, I. and Moulin, C. | 2002 | TOMS and METEOSAT satellite records of the variability of Saharan dust transport over the Atlantic during the last two decades (1979–1997). <i>Geophys. Res. Lett.</i> , 29 , doi: 10.1029/2001GL013767 |

- Chiapello, I., Moulin, C. and Prospero, J. M. 2005 Understanding the long-term variability of African dust transport across the Atlantic as recorded in both Barbados surface concentrations and large-scale Total Ozone Mapping Spectrometer (TOMS) optical thickness. *J. Geophys. Res.*, **110**, D18S10, doi: [10.1029/2004JD005132](https://doi.org/10.1029/2004JD005132)
- Danielsen, E. F. 1975 'The relationship between severe weather, major dust storms and rapid large-scale cyclogenesis, Parts I and II. Subsynoptic Extratropical Weather Systems: Observations, Analysis, Modeling, and Prediction'. Pp. 215–241 in *Notes From a Colloquium: Summer 1974, Vol. II.*, National Center for Atmospheric Research, Boulder, CO, USA
- Davis, C. A. and Emanuel, K. A. 1991 Potential vorticity diagnostics of cyclogenesis. *Mon. Weather Rev.*, **119**, 1929–1953
- Davis, C. A., Grell, E. D. and Shapiro, M. A. 1996 The balanced dynamical nature of a rapidly intensifying oceanic cyclone. *Mon. Weather Rev.*, **124**, 3–26
- Evan, A. T., Heidinger, A. K. and Knippertz, P. 2006 Analysis of winter dust activity off the coast of West Africa using a new 24-year over-water AVHRR satellite dust climatology. *J. Geophys. Res.* in press
- Fink, A. H. and Knippertz, P. 2003 An extreme precipitation event in southern Morocco in spring 2002 and some hydrological implications. *Weather*, **58**, 377–387
- Franzén, L. G., Hjelmsroos, M., Källberg, P., Rapp, A., Mattsson, J. O. and Brorström-Lundén, E. 1995 The Saharan dust episode of south and central Europe, and northern Scandinavia, March 1991. *Weather*, **50**, 313–318
- Ginoux, P., Prospero, J. M., Torres, O. and Chin, M. 2004 Long-term simulation of global dust distribution with the GO-CART model: Correlation with North Atlantic Oscillation. *Environ. Modelling & Software*, **19**, 113–128
- Griffiths, J. F. and Soliman, K. H. 1972 'The northern desert (Sahara)'. Pp. 75–132 in *Climates of Africa*, volume 10 of *World Survey of Climatology*, H. E. Landsberg (Ed.), Elsevier, New York, NY, USA
- Hoskins, B. J., McIntyre, M. E. and Robertson, A. W. 1985 On the use and significance of isentropic potential vorticity maps. *Q. J. R. Meteorol. Soc.*, **111**, 877–946
- Jankowiak, I. and Tanré, D. 1992 Satellite climatology of Saharan dust outbreaks: Method and preliminary results. *J. Climate*, **5**, 646–656
- Kalu, A. E. 1979 'The African dust plume: Its characteristics and propagation across West Africa in winter'. Pp. 95–118 in *Saharan Dust: Mobilization, Transport and Deposition*. C. Morales (Ed.), John Wiley and Sons, Chichester, UK
- Knippertz, P. 2005 Tropical–extratropical interactions associated with an Atlantic tropical plume and subtropical jet streak. *Mon. Weather Rev.*, **133**, 2759–2776
- Knippertz, P. and Martin, J. E. 2005 Tropical plumes and extreme precipitation in subtropical and tropical West Africa. *Q. J. R. Meteorol. Soc.*, **131**, 2337–2365
- 2006 A Pacific moisture conveyor belt and its relationship to a significant precipitation event in the semi-arid southwestern USA. *Weather and Forecasting* in press
- McGuirk, J. P., Thompson, A. H. and Smith, N. R. 1987 Moisture bursts over the tropical Pacific Ocean. *Mon. Weather Rev.*, **115**, 787–798
- Martin, J. E. and Otkin, J. A. 2004 The rapid growth and decay of an extratropical cyclone over the central Pacific Ocean. *Weather and Forecasting*, **19**, 358–376
- Mecikalski, J. R. and Tripoli, G. J. 1998 Inertial available kinetic energy and the dynamics of tropical plume formation. *Mon. Weather Rev.*, **126**, 2200–2216
- Moulin, C., Lambert, C. E., Dulac, F. and Dayan, U. 1997 Control of atmospheric export of dust from North Africa by the North Atlantic Oscillation. *Nature*, **387**, 691–694
- Prodi, F. and Fea, G. 1979 A case of transport and deposition of Saharan dust over the Italian peninsula and southern Europe. *J. Geophys. Res.*, **84**, 6951–6960
- Prospero, J. M. and Carlson, T. N. 1981 Saharan air outbreaks over the tropical North Atlantic. *Pure Appl. Geophys.*, **119**, 677–691
- Prospero, J. M., Ginoux, P., Torres, O., Nicholson, S. E. and Gill, T. E. 2002 Environmental characterization of global sources of atmospheric soil dust identified with the Nimbus 7 total ozone mapping spectrometer (TOMS) absorbing aerosol product. *Rev. Geophys.*, **40**(1), 1002, doi: [10.1029/2000RG000095](https://doi.org/10.1029/2000RG000095)
- Roebber, P. J. 1984 Statistical analysis and updated climatology of explosive cyclones. *Mon. Weather Rev.*, **112**, 1577–1589

- Smith, R. K. and Reeder, M. J. 1988 On the movement and low-level structure of cold fronts. *Mon. Weather Rev.*, **116**, 1927–1944
- Swap, R. S., Ulanski, S., Cobett, M. and Garstang, M. 1996 Temporal and spatial characteristics of Saharan dust outbreaks. *J. Geophys. Res.*, **101**, 4205–4220
- Thorncroft, C. D. and Flocas, H. A. 1997 A case study of Saharan cyclogenesis. *Mon. Weather Rev.*, **125**, 1147–1165
- Tompkins, A. M.,
Diongue-Niang, A.,
Parker, D. J. and
Thorncroft, C. D. 2005 The African easterly jet in the ECMWF integrated forecast system: 4D-Var analysis. *Q. J. R. Meteorol. Soc.*, **131**, 2861–2886
- Trenberth, K. E. 1992 ‘Global analyses from ECMWF and atlas of 1000 to 10 mb circulation statistics’. NCAR Tech Note, NCAR/TN-373+STR, (NTIS PB92-218718/AS), National Center for Atmospheric Research, Boulder, CO., USA
- Washington, R. and Todd, M. C. 2005 Atmospheric controls on mineral dust emission from the Bodélé Depression, Chad: The role of the low level jet. *Geophys. Res. Lett.*, **32**, L17701, doi: 10.1029/2005GL023597
- Washington, R., Todd, M.,
Middleton, N. J. and
Goudie, A. S. 2003 Dust-storm source areas determined by the Total Ozone Monitoring Spectrometer and surface observations. *Annals Assoc. Am. Geogr.*, **93**, 297–313
- Wernli, H., Dirren, S.,
Liniger, M. A. and Zillig, M. 2002 Dynamical aspects of the life cycle of the winter storm ‘Lothar’ (24–26 December 1999). *Q. J. R. Meteorol. Soc.*, **128**, 405–429
- WMO 1995 *Manual on codes. International Codes, Vol. I.1, Part A—Alphanumeric Codes*. WMO-No. 306. World Meteorological Organization, Geneva, Switzerland